Pseudopotential-based multiband k p method for ; 250 000-atom nanostructure systems

Lin-Wang Wang* and Alex Zunger
National Renewable Energy Laboratory, Golden, Colorado 80401
~Received 4 June 1996!

The electronic structure of quantum wells, wires, and dots is conventionally described by the envelope-function eight-band **k p** method ~the ''standard **k p** model''! whereby coupling with bands other than the highest valence and lowest conduction bands is neglected. There is now accumulated evidence that coupling with other bands and a correct description of far-from-G bulk states is crucial for quantitative modeling of nanostructure. While multiband generalization of the **k p** exists for *bulk* solids, such approaches for *nanostructures* are rare. Starting with a pseudopotential plane-wave representation, we develop an efficient method for electronic-structure calculations of nanostructures in which ~i! multiband coupling is included throughout the Brillouin zone and ~ii! the underlying bulk band structure is described correctly even for far-from-G states. A previously neglected interband overlap matrix now appears in the **k p** formalism, permitting correct intervalley couplings. The method can be applied either using self-consistent potentials taken from *ab initio* calculations on prototype *small* systems or from the empirical pseudopotential method. Application to both short- and long-period $(\mathrm{GaAs})_p/(\mathrm{AlAs})_p$ superlattices ~SL! recovers ~i! the bending down ~''deconfinement''! of the G(G) energy level of ~001! SL at small periods p; ~ii! the type-II–type-I crossover at $p \simeq 8$ SL, and ~iii! the even-odd oscillation of the energies of the $R/X(L)$ state of ~001! SL and G(L) state of ~111! SL. Introducing a few justified approximations, this method can be used to calculate the eigenstates of physical interest for large nanostructures. Application to spherical GaAs quantum dots embedded in an AlAs barrier ~with ; 250 000 atoms! shows a type-II–type-I crossover for a dot diameter of 70 Å, with an almost zero G-X repulsion at the crossing point. Such a calculation takes less than 30 min on an IBM/6000 workstation model 590. @S0163-1829~96!03439-X#

I. INTRODUCTION: THE NEED FOR A BETTER k p METHOD FOR NANOSTRUCTURES

Most electronic-structure calculations of semiconductor nanostructures are performed today using the ''standard model,'' namely, the four-band ~eight-band, including spin! **k p** envelope-function approach.[1–8] In this approach the electronic states *cG¬0¬TD (k)Tj /F9¬1¬Tf*

respect to direct diagonalization,[16] ~v! significant *quantitative* underestimation by the standard model of the position of the second heavy-hole state ~hh2! and split-off bands for binding energies > 200 meV[16], and incorrect out-of-plane dispersion and incorrect position p of the avoided crossing,[16] ~vi! omission of the spin splitting for the in-plane dispersion of the valence bands, and ~vii! overestimation of the mass anisotropy $m_i/m_\cdot$ at Γ for both electrons and holes.[16]

While it was generally expected[4] that the standard model will fail for small nanostructures ~e.g., short-period superlattices!, direct diagonalization studies[16] have shown that the situation is not so simple. For example, the first heavy-hole ~hh1! and the first light-hole ~lh1! valence-band energies of $(\mathrm{GaAs})_p/(\mathrm{AlAs})_p$ ~001! superlattices are accurately described by the standard model even down to the $p=1$ monolayer superlattice limit, while the conduction bands folded from Γ and X are poorly described even at $p \sim 20$. This is so because the standard **k p** model describes poorly the energy of the zinc-blende X_{1c} state which has a significant projection in the superlattice conduction band. On the other hand, the coupling between the folded X_{1v} and Γ_{15v} states at the superlattice *valence* band ~also described poorly! happens to be weak, so its misrepresentation is inconsequential. Incorrect description of intervalley coupling of folded states is also the reason for the significant errors made by the **k p** model in describing the values of the superlattice miniband effective-mass tensor, the deformation potential,[17] and the wave-function localization[18] of InP/GaP superlattices.

In isolated GaAs or Si quantum *films*, the direct diagonalization approach reveals a thickness-independent ''zero confinement state'' at the valence-band maximum,[19] which is missed by the standard **k p** model. Furthermore, in isolated quantum *dots* of Si and CdSe,[20–22] accurate description of the observed band gap vs size dependence requires a many-band approach.

Common to all of the failures of the standard model are ~i! the neglect of intervalley ~e.g., Γ-X) couplings and ~ii! the poor description of the bulk band structure over most of the first Brillouin zone. While both goals can be accomplished by the plane-wave direct diagonalization approach using a pseudopotential description of the nanostructure potential $V^{\mathrm{NS}}(r)$ @Eqs. ~2! and ~3!#, the number N_k of the plane-wave basis functions increases in this approach too rapidly with system size. More importantly, there is no simple physical principle ~other than a systematic change of N_k) telling us how to reduce the size of the basis set without introducing a significant error. Thus only $O(10^3)-O(10^4)$ atom systems can be conveniently described, even using linear-in-size matrix diagonalization techniques in which only eigenvalues in a desired energy window are sought.[14] There are some important questions in nanostructure physics that require consideration of larger numbers of atoms. For example, while in ~i! ~001! $(\mathrm{AlAs})_p/(\mathrm{GaAs})_p$ *superlattices*, the type-II–type-I transition occurs at[23] $p_c \sim 8-11$ ~32–44 atoms/supercell!, and in ~ii! AlAs-embedded GaAs *wire* it occurs at the diameter $D>52$ Å (; 2000 atoms/supercell!, in ~iii! AlAs-embedded GaAs *dots*, this transition is estimated to occur at $D>70$ Å (; 250 000 atoms/supercell!, well outside the reach of direct diagonalization approach. The representation of Eq. ~1! ~where bulk Bloch functions $\{u_{n,\Gamma}\}$ are used instead of individual plane waves! is more attractive for such 10^4-10^6 atom systems, since in this limit the number of basis functions used to describe the envelope function $F_n(r)$ can be *system-size independent*. More specifically, one could limit the sum to those (n,k) values that are physically needed to give good convergence, rather than using all states. However, the standard **k p** method cannot be used here since it does not describe the Γ and X states together, hence it

where m_0 is the real electron mass. The momentum matrix element is

$$P^A(n,m) = \langle u^A_{m,0} | \hat{p} | u^A_{n,0} \rangle. \quad (8)$$

Thus, given the $k = 0$ eigenvalues $\{\varepsilon^A_{n,0}\}$ and the $k = 0$ momentum matrix $\{P^A(n,m)\}$ one can solve Eq. (6) and find the full $k \neq 0$ dispersion relation $\varepsilon^A_{n,k}$ over the first BZ.

Due to the completeness of the basis $u^A_{n,0}$, we have

$$\hat{H}^A | u^A_{n,0} e^{i\mathbf{k}\cdot\mathbf{r}} \rangle = \sum_{m=1}^{N_m} H^A

$$S^A(p,m,k) = \int u_p^A(r)\, u_m^{A*}(r)\, w(r)\, e^{2i\mathbf{k}\cdot\mathbf{r}}\, d^3r \qquad (18)$$

and the *structure factor* of material A is

$$C^A(k) = \frac{1}{N_c}\sum_{R\in A} e^{2i\mathbf{k}\cdot\mathbf{R}}. \qquad (19)$$

Note that because of the factor $w(r)\exp(2i\mathbf{k}\cdot\mathbf{r})$, we have $S^A(p,m,k) \neq \delta_{p,m}$ despite the orthonormality between u_p^A and u_m^A. The same formalism gives for the matrix elements of part B of the Hamiltonian in the B-type basis set

$$H_B^{\mathrm{PB}}(mk',nk) = \frac{1}{N_c}\langle u_m^B e^{i\mathbf{k}'\cdot\mathbf{r}} | \hat{H}^{\mathrm{PB}} | u_n^B e^{i\mathbf{k}\cdot\mathbf{r}}\rangle = \sum_{p=1}^{N_m} H^B(n,p,k) S^B(p,m,k'-k) C^B(k'-k). \qquad (20)$$

In Eqs. (17) and (20), the subscripts A or B denote the basis functions, while the superscripts PA and PB denote the Hamiltonian defined in Eq. (11). Because $\{u_n^A(r)\}$ and $\{u_m^B(r)\}$ each represent a complete basis, they can be inter-transformed via a unitary transformation

$$u_n^A(r) = \sum_{m=1}^{N_b} \tilde{U}(m,n)\, u_m^B(r) \qquad (21)$$

and

$$\tilde{U}(m,n) = \int_{\mathrm{PC}} u_m^{B*}(r)\, u_n^A(r)\, d^3r \qquad (22)$$

where PC stands for integration over one primary cell. Thus the matrix element H_A^{PB} of the Hamiltonian $\hat{H}^{\mathrm{PB}}$ in an A-type basis of Eq. (12) can be obtained from H_B^{PB} in Eq. (20) by

$$H_A^{\mathrm{PB}}(mk',nk) = \frac{1}{N_c}\langle u_m^A e^{i\mathbf{k}'\cdot\mathbf{r}} | \hat{H}^{\mathrm{PB}} | u_n^A e^{i\mathbf{k}\cdot\mathbf{r}}\rangle = \sum_{p',p=1}^{N_b} \tilde{U}^*(p',m) H_B^{\mathrm{PB}}(p'k',pk) \tilde{U}(p,n). \qquad (23)$$

Finally, the matrix elements $H_A^{\mathrm{NS}}(mk',nk)$ in Eq. (15) of the total nanostructure Hamiltonian in an A-type basis is

$$H_A^{\mathrm{NS}}(mk',nk)$$

the eigenfunction equation error.

~c! The transformation matrix $\widetilde{U}(m,n)$ between $u_n^A(r)$ and $u_m^B(r)$ @Eqs. ~21! and ~22!# is not unitary if N_b is truncated. In this case, $\$u_n^B(r)\%$ cannot be connected exactly to $\$u$

similar to that obtained by exact direct diagonalization, but that when less than 15 G Bloch bands are used, the band structure suddenly becomes much worse. Note in particular how for 8 or 5 G bands the energy of the X_{1c} band as obtained in **k p** is ; 20 eV too high and the curvature ~hence effective mass! of the valence band reverses sign. The situation is similar for AlAs and Si ~not shown!.

To show how many G Bloch states $\$u_{n\mathsf{G}}\%$ are needed to describe the directly calculated X Bloch state u_{nX} of bulk GaAs, we plot in Fig. 5 the closure quantity

$$P_n(N_b) = \sum_{m=1}^{N_b} |\langle u_{m\mathsf{G}} | u_{nX} \rangle|^2 \qquad (25)$$

for $n = 1, \ldots, 8$, where $n = 1$ is the lowest X_{1v} valence band, $n = 4$ is the highest X_{3v} valence band, and $n = 5,6,7,8$ are the lowest four conduction bands, respectively. Here $P_n(N_b) = 1$ means that the nth X-point Bloch state can be described exactly by the first N_b G-point Bloch states. As we can see from Fig. 5, there is a sudden drop of $P_n(N_b)$ for N_b less than 15. This is consistent with the band-structure results in Figs. 3 and 4. The situation is qualitatively similar for AlAs and Si ~not shown!. We conclude that 15 zero-wave-vector bulk bands ~30 with spin! are needed for a *qualitatively* correct description of the dispersion relation in bulk solids, while about 150 bands are needed for a *quantitatively* converged (< 1 2 2 meV! description. We will eventually @Sec. IV A# find ways to obtain a *quantitative* description using only 15 bands.

C. k p for GaAs $_p$ /

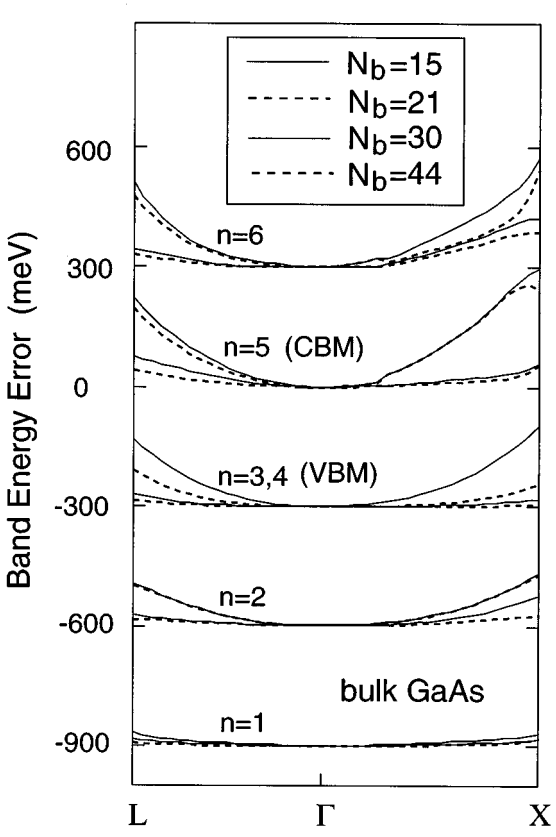

FIG. 4. Errors $e_n(N_b)$

connection error ~c! in our final **k p** nanostructure calculation will be ; 18 meV. There, a better approximation of $\tilde{U}(n,m)$, instead of $\tilde{U}(n,m)=\delta_{n,m}$, will be used. As a result, the unitary connection error ~c! will be much smaller than 18 meV.#

Convergence of **k p** superlattice eigenvalues with N_b are shown in Figs. 7–9. Here the $N_b=65$ results serve as the references and $N_m=369$ and $\tilde{U}(n,m)=\delta_{n,m}$ are used for all calculations. When N_b changes from 65 to 44, the X-folded conduction-band $\Gamma(X_z)$ state moves up by more than 50 meV ~this is consistent with the bulk band-structure errors reported in Figs. 3–4!. When N_b is further reduced, the $\Gamma(X_z)$ state continues to move up. From $N_b=21$ to 15, the change is relatively small, while from $N_b=15$ to 11, the change is large. Similar trends in the error of the L-folded conduction state X/R are shown in Fig. 9. The large change below $N_b=15$ is consistent with the results found for the bulk band structure ~Figs. 3 and 4! and $P_n(N_b)$ ~Fig. 5!. We see that the basis-set truncation error in superlattice energies parallels the errors in the bulk. The above analysis further shows that $N_b=15$ is a turning point, i.e., for N_b , 15 Γ bands, the band structure cannot be described *even qualitatively*. Thus, in the rest of this paper, we will use $N_b=15$ Γ bands for GaAs and AlAs. We next develop a formalism appropriate to many-band coupling where a *truncated* $N_b=N_m=15$ basis set is used.

IV. THE FINITE-N_b FORMALISM

A. Fixing the k p bulk band-structure error

The above study shows that the **k p** error in the bulk band structure carries over to the nanostructure. So our first task here is to reduce the **k p** bulk band-structure error ~a! of band-edge states for $N_b=15$ to less than 5 meV from ; 300 meV ~see the X and L points in Figs. 3 and 4!.

The effects of removing higher-energy bands on the energies of lower states can be described as Löwdin folding.[30] This is a procedure that modifies the elements of the Hamiltonian matrix so that the eigenvalues of the submatrix spanned by the lower-energy states equal the eigenvalues of the original full matrix. As a result, the effects of the truncation to finite N_b bands can be compensated by a replacement of the bare electronic mass m_0 in Eq. ~7! with ''mass parameters'' m_n^A. Furthermore, to fit the dispersion in both the Γ-X and the Γ-L directions, we need a nonspherical correction term. This term comes from a higher-order Löwdin folding effect ~i.e., a fourth-order term in k): $f(k)=3(k_x^4+k_y^4+k_z^4)-k^4$. @Here $f(k)=0$ for the ~111! direction and $f(k)=2k^4$ for the ~001! direction.# Thus we have revised Eq. ~7! to

$$H^A(n,m,k)=\left[e_{n,0}^A+\frac{1}{2m_n^A}k^2+a_n^A f(k)\right]\delta_{n,m}-i\mathbf{k}\cdot\mathbf{P}^A(n,m), \quad (26)$$

where $e_{n,0}^A$ and $P^A(n,m)$ are unchanged from Eq. ~7!. For $N_b=15$, due to the degeneracy, we have eight independent

m_n^A values and eight independent a_n^A values. These are used to fit the two lowest conduction-band and the highest valence-band energies. The fitted **k p** bulk band structures of GaAs and AlAs are shown in Figs. 10~a! and 10~b!, while the errors, relative to a direct plane-wave diagonalization calculation, are shown in Fig. 11. The fitting parameters $m_n^{A(B)}$ and $a_n^{A(B)}$ are listed in Table I. The $m_n^{A(B)}$'s are close to 1 and the $a_n^{A(B)}$'s are small. The physically important bottom of conduction-band states (n 5 5 in Fig. 11!, especially near the Γ, X, L points, have typical errors of only ; 3 meV, much better than the unfitted error of ; 300 meV seen in Figs. 3~a! and 4.

In this work we have calculated the quantities $e_{n,0}^A$ of Eq. ~7!, $P^A(n,m)$ of Eq. ~9!, and $S^A(n,m,k)$ of Eq. ~18! using the empirical pseudopotential plane-wave method[25,26] ~so as to ensure accurate eigenenergies and wave functions!. These quantities can also be obtained from self-consistent calculations such as the local-density approximations ~LDA! provided that the LDA errors in the band structure $e_{n,0}^A$ were subsequently corrected. If nonlocal pseudopotentials are used in the LDA or in the empirical pseudopotential calculation,[22] its effects could also be represented by the mass parameters $\$m_n\%$ and the $f(k)$ term in Eq. ~26!.

B. Fixing the unitary connection error

Having fixed the bulk band structure, we return now to the eigenfunction equation error ~b! and unitary connection error ~c!. As shown in Fig. 6, the eigenfunction equation error ~b! is small, at least when N_b 5 N_m 5 65. Thus no attempt is made to correct it here. We will use N_b 5 N_m 5 15 throughout the rest of the work. As also shown in Fig. 6, the unitary connection error ~c! could be large if we let $\tilde{U}(n,m)$ be $\delta_{n,m}$. The $\tilde{U}(n,m)$ calculated from Eq. ~22! is not unitary for truncated N_b, thus it cannot be used directly. Appendix B describes a simple procedure ~Löwdin orthogonalization!, with minimum modifications of $\tilde{U}(n,m)$, converting it to an unitary matrix. The resulting $\tilde{U}(n,m)$ is then used in Eq. ~23!. Treated in this way, the unitary connection error ~c! becomes rather small.

C. A special method to calculate $S^{A\,B}\ \ n,m,k$

The overlap matrix $S^{A(B)}(n,m,k)$ in Eqs. ~17! and ~20! needs to be calculated from its definition Eq. ~18! for all the nanostructure wave vector k inside the 2BZ. Direct calculation of the overlap matrix could be time consuming. For one-dimensional superlattices one can use a numerically accurate interpolation scheme as done in Sec. III. However, for three-dimensional systems ~e.g., quantum dots!, $S^{A(B)}(n,m,k)$ needs to be precalculated for numerous **k** values. In the following, we will introduce an alternative, easier approach to calculate this overlap matrix.

Substituting the Fourier expansion $w(r)$ 5 @V_c/

both, so as to avoid double counting. To ensure that both choices yield the same result and, more importantly, that the $k = -k_X$ point ~when $-X$ is chosen! couples properly with the $k = k_X - 2p/L$ points ~where L is the length of the system!, we need $u^A_{n,-X}$ to behave like $u^A_{n,X}\exp(i2k_X r)$. More precisely, we need to have

$$u^A_{n,-G/2}(r + L) = e^{i\theta_n}$$

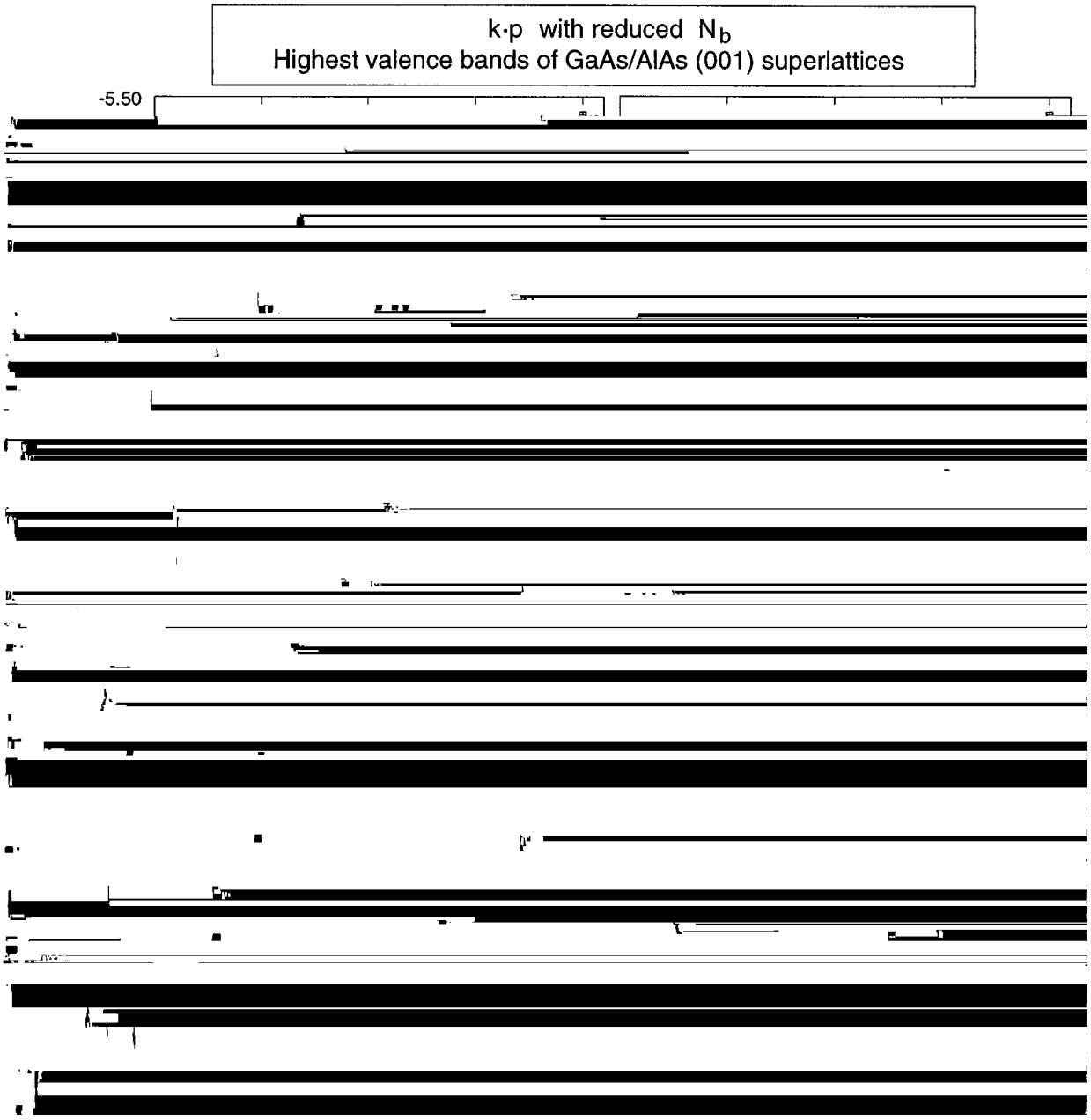

FIG. 8. Effects of reducing N_b on the **k p** GaAs/AlAs ~001! superlattice valence bands. The calculation conditions are the same as in Fig. 7. The squares are the same as the squares in Fig. 6~b!.

$$U^A\sim n,m,2\,G/2!5\,e^{iu_m}\Big(_{p51}^{N_b}U^A\sim p,m,G/2!\mathcal{O}^A\sim p,n,2\,G!. \tag{31}$$

This equation is automatically satisfied for $N_b5\,`$, but is no longer exactly true for a finite N_b. To satisfy it for $G/25k_X$ and for $G/25k_L$, we need to modify $\mathcal{O}^{A(B)}(n,m,2k_X)$ and $\mathcal{O}^{A(B)}(n,m,2k_L)$ from their original values given by Eq. ~28!. This modification is described in Appendix B. For $\mathcal{O}^{A(B)}(n,m,G)$ evaluated at other **G**'s, the direct result of Eq. ~28! could be used in Eq. ~27! without any change.

Once $\tilde{U}(n,m)$ and $\mathcal{O}^{A(B)}(n,m,G)$ are obtained, the Hamiltonian matrix $H_A^{\rm NS}(mk8,mk)$ can be readily calculated from Eq. ~24!. However, because the approximations are made in conjunction with the finite N_b, the $H_A^{\rm NS}(mk8,mk)$ calculated from Eqs. ~24!, ~23!, ~20!, and ~17! is not exactly Hermitian. This non-Hermitian error can be measured by

$$a5\Big(_{mk8,nk}\mathbb{U}H_A^{\rm NS}\sim mk8,nk!2\,H_A^{\rm NS*}\sim nk,mk8!\mathbb{U}\Big)^{\gamma}\Big(_{mk8,nk}\mathbb{U}H_A^{\rm NS}\sim mk8,nk!\mathbb{U}. \tag{32}$$

We find that a is of the order of $0.53\,10^{23}$ for our GaAs/AlAs systems. @Had we used $\tilde{U}(n,m)5d_{n,m}$, this a would be ten times larger.# To circumvent this non-

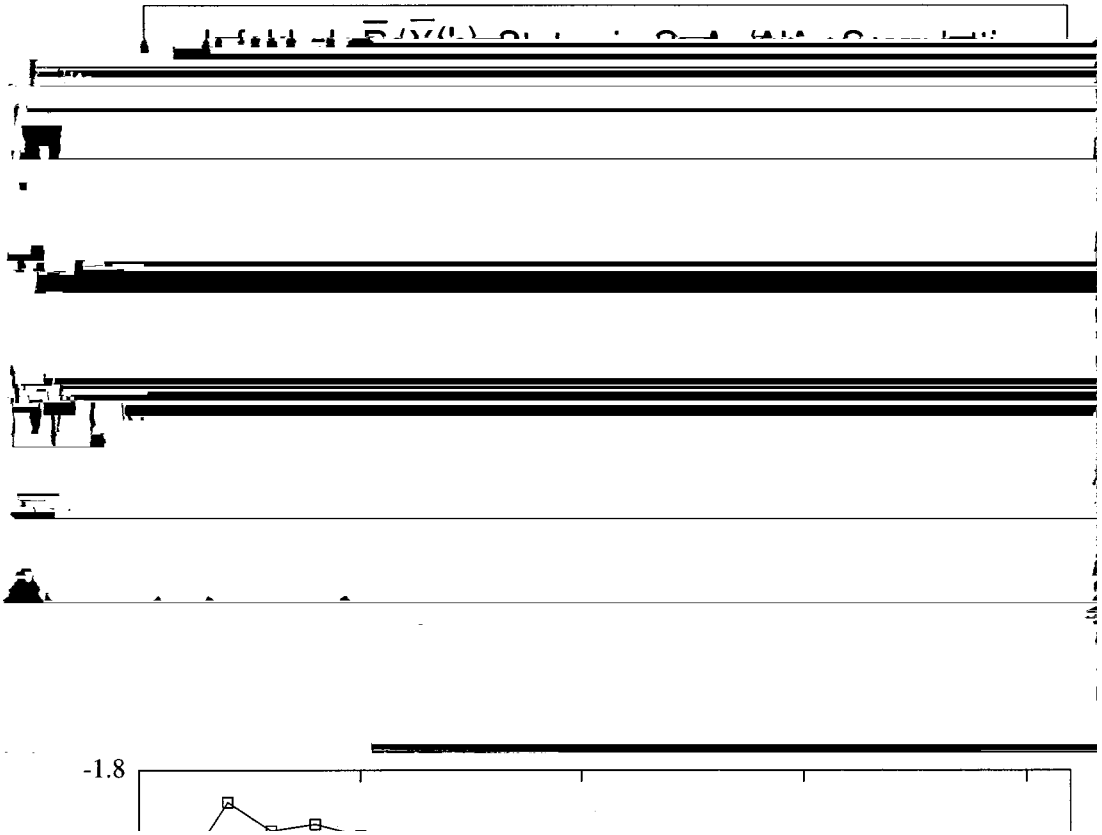

FIG. 9. Effects of reducing N_b on the **k p** GaAs/AlAs ~001! superlattice $\overline{R/X(L)}$ conduction bands. The calculation conditions are the same as in Fig. 7.

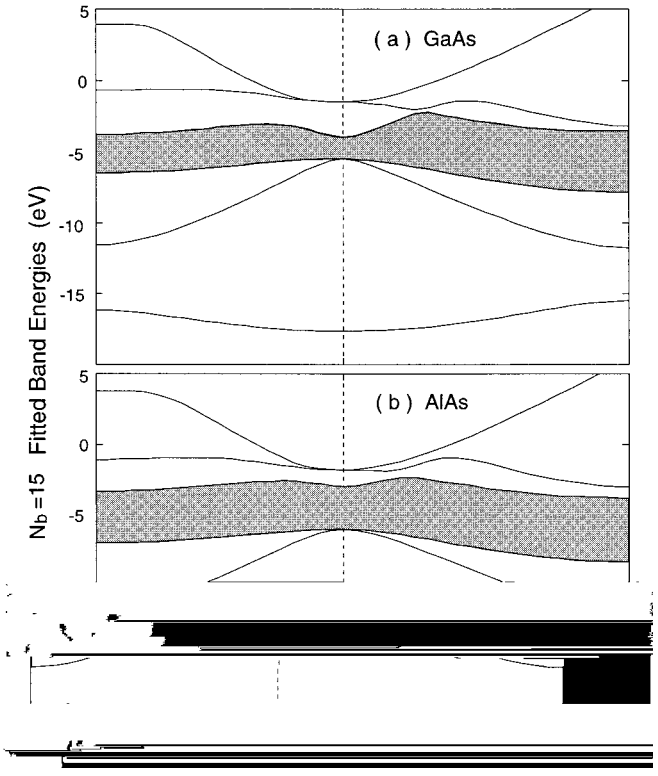

FIG. 10. Fitted **k p** band structures of ~a! bulk GaAs and ~b! AlAs using $N_b 5 15$.

Hermitian problem, we simply symmetrize the matrix as $@H_A^{\mathrm{NS}}(mk8,nk) 1 H_A^{\mathrm{NS}*}(nk,mk8)#/2$ and then diagonalize the symmetrized matrix.

D. Choice of the interfacial potential

In Sec. IV C, the calculation of $S^{A(B)}(n,m,k)$ required a smooth $w(r)$ function @with zero $W(k)$ outside 2BZ#. However, in reality, the interface could be sharper than $V_w^{\mathrm{NS}}(r)$ calculated from such $w(r)$ via Eq. ~10!. Here we will introduce an interfacial potential to restore the sharpness of the interface from $V_w^{\mathrm{NS}}(r)$:

$$V^{\mathrm{IF}}\sim r! 5 V_{\mathrm{sharp}}^{\mathrm{NS}}\sim r! 2 V_w^{\mathrm{NS}}\sim r!, \qquad \sim 33!$$

where the superscript IF stands for interface.

$V^{\mathrm{IF}}(r)$ defined in Eq. ~33! is localized at the interface and is the interfacial potential for the whole system. We first break it down to its constituents belonging to each primary cell of the interface. Let us first define an interface primary cell of $A(B)$ as a primary cell for material $A(B)$ that has at least one $B(A)$ neighboring primary cell. We will use $\mathcal{R}$ to denote one interfacial primary cell and its position and $A/I(B/I)$ to denote the domain of the interfacial primary cell. To break down $V^{\mathrm{IF}}(r)$, we have

$$V^{\mathrm{IF}}\sim r! 5 \Big(_{\mathcal{R}\in A/I} V^{A}\sim r 2 \mathcal{R},\mathcal{R}! 1 \Big(_{\mathcal{R}\in B/I} V^{B}\sim r 2 \mathcal{R},\mathcal{R}!, \qquad \sim 34!$$

where $V^{A(B)}(r,\mathcal{R})$ is the interfacial potential contribution from interfacial primary cell $\mathcal{R}$. It should only depend on the

local atomic arrangements surrounding $\mathcal{R}$. We will further break down $V^A(r,\mathcal{R})$ into its contribution from the neighboring B-type primary cells. Suppose that an A-type primary cell $\mathcal{R}$ has $m(\mathcal{R})$ neighboring primary cells of type B; then

$$V^A(r,\mathcal{R}) = \sum_{i=1}^{m(\mathcal{R})} V^A_{g_i}(r), \qquad (35)$$

where the subscript g_i indicates the position of the neighboring primary cell. Considering only the nearest neighbors of a fcc primary cell of the zinc-blende lattice, we have 12 possible position g_i. Their $V^A_{g_i}(r)$ are connected by symmetry operations so only one of them needs to be studied here (say, $g_i = xy$, the neighboring position of (110)$a/2$).

Suppose the matrix element of $V^A_{g_i}(r)$ in the A-type Bloch basis is

$$H^A_{g_i}(m,n,k) = \int u^{A*}_m(r) V^A_{g_i}(r) u^A_n(r) e^{2i\mathbf{k}\cdot\mathbf{r}} d^3r; \qquad (36)$$

then the Hamiltonian matrix of $V^{\mathrm{IF}}(r)$ under this basis is

$$\begin{aligned} H^{\mathrm{IF}}_A(mk\alpha,nk') = {} & \frac{1}{N_c} \int u^A_m e^{i\mathbf{k}'\cdot\mathbf{r}} V^{\mathrm{IF}}(r) u^A_n e^{i\mathbf{k}\cdot\mathbf{r}} \\ & = \sum_{\mathcal{R}\in A/I} \sum_{i=1}^{m(\mathcal{R})} H^A_{g_i}(m,n,k\alpha) \frac{1}{N_c} e^{2i(k-k')\cdot\mathcal{R}} \\ & - \sum_{\mathcal{R}\in B/I} \sum_{i=1}^{m(\mathcal{R})} H^{B\alpha}_{g_i}(m,n,k\alpha) \\ & \times \frac{1}{N_c} e^{2i(k-k')\cdot\mathcal{R}}. \end{aligned} \qquad (37)$$

Here $H^{B\alpha}_{g_i}$ is $H^B_{g_i}$ in the u^A_n basis (instead of the u^B_n basis!); thus

$H^{B\alpha}_{g_i}(n,m,k)$

V. RESULTS FOR NANOSTRUCTURES USING THE MULTIBAND k p METHOD

A. Superlattices in the u_0 represenation

The comparisons between the multiband **k p** and the direct plane-wave diagonalization results for the superlattice energy levels are shown in Figs. 12 and 13. As we can see, the trends in the results of the direct diagonalization and the multiband **k**

components in Eq. ~1! or ~12!. In practice, we will select a fixed number of **k** points around the bottom of the physically interesting band-structure valleys ~e.g., Γ, X, and L), regardless of the size of the nanostructure.

In Fig. 14 we show the results for the ~001! $(\mathrm{GaAs})_p/(\mathrm{AlAs})_p$ superlattices using a fixed number of **k** points in the basis set of Eq. ~12!. As can be seen, if we have $\Delta k = (-5, \ldots, 0, \ldots, 5)(2\pi/L)$ ~where L is the length of the supercell! around Γ ~i.e., $k = k_\Gamma + \Delta k$) and $\Delta k = (-3, \ldots, 0, \ldots, 3)(2\pi/L)$ around X, then the fixed **k**-point basis introduces an error of only 3 meV for the band-edge Γ- and X-folded states. Thus, in a three-dimensional ~quantum dot! calculation, we could use the $(-5, \ldots, 5)$ and $(-3, \ldots, 3)$ as the cutoff spherical diameters around Γ and X to select **k** points in the basis. A similar diameter exists for the L point. Using these diameters, we need typically only 1000–2000 **k** points for a three-dimensional system.

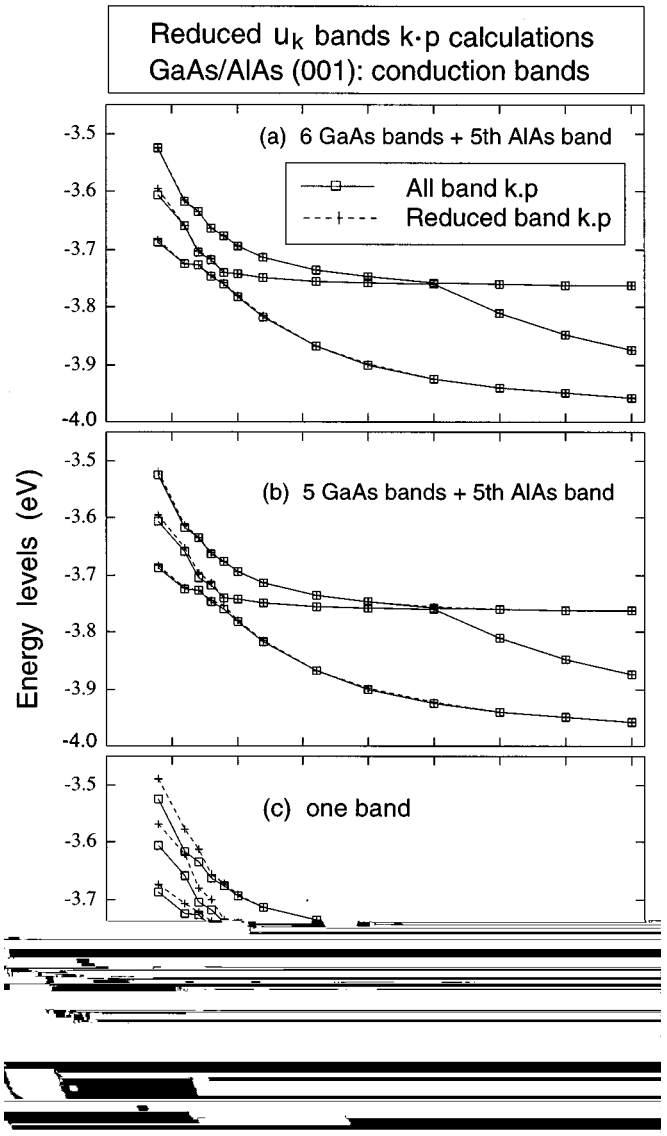

FIG. 15. Reduced band **k p** GaAs/AlAs ~001! superlattice conduction-band energy levels ~dashed lines and pluses! compared with the all band **k p** results ~solid lines and squares!. The one-band calculation in ~c! uses the fifth GaAs state for **k** points close to G and the fifth AlAs state for **k** points close to *X*.

to the G_{1c}(GaAs) state.[23] At the ~anti!crossing point, there could be a G-*X* coupling. The computational difficulty of this problem is that in a supercell description, very thick AlAs barriers are needed to avoid overlap of neighboring GaAs quantum-dot wave functions.[23] We have calculated GaAs quantum dots up to 160 Å in diameter, while the size of AlAs matrix is kept at 50 3 50 3 50 primary cells. This corresponds to a 250 000 atoms.

The $C^{A(B)}(k)$ structure factor defined in Eq. ~19! and its counterparts for the interfacial potentials in Eq. ~37! were calculated using fast Fourier transforms. **k**-point selection spheres are placed at the G point and the three *X* points using slightly larger diameters of (2 6, . . . ,0, . . . ,6! and (2 4, . . . ,0, . . . ,4! than the ones used in Fig. 14. There are 2260 **k** points in total. When the selected **k** point is inside the sphere of the G point, $u_{5,k}^{\mathrm{GaAs}}$ is used in the basis set. When the selected **k** point is inside the spheres of the *X* point, $u_{5,k}^{\mathrm{AlAs}}$ is used in the basis set. So, the total number of basis function is also 2260. The total CPU time for calculating the matrix $H_a^{\mathrm{tot}}(mk8,nk)$ and diagonalizing it is less than 30 min on an IBM/6000 workstation model 590. The calculation takes about 100 megabyte memory, mainly to host the 2260 3 2260 double precision complex matrix $H_a^{\mathrm{tot}}(mk8,nk)$.[34]

The results are shown in Fig. 16. The crossover diameter between type-I and type-II behavior is found to be 70 Å. However, surprisingly, we find no coupling between the G- and *X*-induced states. Due to the spherical shape of the quantum dot, the three *X*-point states are degenerated. They have a different symmetry representation than the single degenerated G state. Thus the G and *X* states do not couple in this case. To get a G-*X* coupling, some other shapes ~e.g., disk! of the quantum dot, or a spherical dot with an As atom at its origin, is needed. In addition, pressure-dependent rather than size-dependent eigenenergy curves might be needed to find small G-*X* anticrossing since smooth curves are available only in the pressure-dependent case.

VI. COMPARISON WITH OTHER METHODS

In this section we summarize briefly the similarities and differences of the current method with alternative approaches.

A. Comparison with the standard k p model

Formally, our method differs from the standard **k p** model by the use of a u_0 basis of pure *A* @Eq. ~12!# leading to the appearance of an overlap matrix $S^A(n,m,k)$ @Eq. ~18!# in the evaluation of the Hamiltonian matrix in Eq. ~17!. Besides, due to the use of many bands, our wave vector **k** is restricted to reside inside the BZ. Thus, unlike the standard **k p** model, our Hamiltonian equation cannot be formally changed to a differential equation.

Practically, we include many-band ~15 for GaAs/AlAs! rather than four-band coupling and a bulk band structure that is accurate over the *entire* BZ. As a result, we are able to reproduce the energetic features of short period superlattices ~Figs. 12 and 13! missed by the standard model.[16]

B. Comparison with direct plane wave diagonalization

In the direct plane-wave diagonalization @Eqs. ~2! and ~3!#, the basis functions are classified according to momentum alone, not band index, so there is no intuitive way to select the variationally most important states. Instead, one has to increase systematically the basis size. In contrast, in the u_0 representation, and more so in the u_k representation, one can preselect basis functions on the basis of their likely coupling in the nanostructure band edge states. This is decided based on the proximity of the energy of a given bulk basis function to the band edges.

We have recently developed the ''folded spectrum method'' ~FSM! ~Ref. 14! to efficiently solve for the band-gap edge states of nanostructures. The FSM provides exact solutions of the plane-wave diagonalization, so the FSM solutions are superior to the current **k p** approach ~if the current **k p** Hamiltonian is developed from the plane-wave pseudopotential Hamiltonian!. The problem with the FSM is that when the system is much larger than a few thousand

atoms, the FSM is too time consuming. In such cases, the current **k p** method can be used as a substitute. The FSM is well suited to solve for random alloys,[35] rough interfaces,[36] and isolated quantum dots.[14,22] In cases of three-dimensional nanostructures with shallow barriers ~e.g., material *A* embedded in material *B* quantum dots!, usually larger systems (. 10 000 atoms! are needed. The current method is designed to solve just such problems.

ACKNOWLEDGMENTS

The authors would like to thank Dr. A. Franceschetti, Dr. S. Froyen, and Dr. D. Wood for many helpful discussions. This work was supported by the office of Energy Research, Material Science Division, U.S. Department of Energy, under Grant No. DE-AC02-83CH10093.

APPENDIX A: CREATING A PLANE-WAVE BASIS FROM A POLYHEDRON

In the conventional plane wave basis calculation of Eqs. ~2! and ~3!, a sphere of radius $G_{\rm cut}=\sqrt{2E_{\rm cut}}$ ~where $E_{\rm cut}=6.5$ Ry! is used to select the plane-wave basis $\{G\}$. This sphere contains 65 plane-wave functions at the $k=\Gamma$ point. When the **k** point moves away from Γ, the number of plane-wave basis functions enclosed within the **k**-centered radius-$G_{\rm cut}$ sphere may also change. The **k p** formalism with $N_b=65$ cannot reproduce this change of the plane-wave basis set. As a result, there is a 20 meV energy difference between the $N_b=65$ **k p** results and the plane-wave calculations at the *X* and *L* points. ~Using a smooth $E_{\rm cut}$ technique described in Ref. 26, the band structure of the plane-wave calculation is smooth, despite the possible sudden change of the number of the plane-wave functions.! We need to eliminate this difference, so that we can produce an exact **k p** result that could be compared with the results of the direct plane-wave diagonalization. To this end, instead of using a conventional $G_{\rm cut}$-radius sphere centered at the **k** point, we will use a special polyhedron zone to select the plane-wave basis. This zone is also centered at the **k** point when **k** is away from Γ. It has a shape of Wigner-Seitz primitive cell of the *real-space* crystal lattice. Thus, its surfaces are parallel to the planes of the reciprocal lattice. When $k=\Gamma$, these surfaces are in the middle of two neighboring parallel reciprocal-lattice planes. The advantage of this special polyhedron zone is that when **k** moves within the first BZ, this polyhedron will not cut through any reciprocal lattice points, thus the plane-wave basis will not be changed. Consequently, the $N_b=65$ **k p** band structure is exactly the same as obtained in direct plane-wave diagonalization. This zone is used only in Sec. III.

APPENDIX B: THE CORRECTION OF $\tilde{U}(n,m)$ AND $O_A(n,m,G)$

In the following, we discuss separately the correction of $\tilde{U}(n,m)$ and the correction of $\mathcal{O}_A(n,m,G)$.

When $N_b=15$, the $\tilde{U}(n,m)$ defined in Eq. ~22! is no longer unitary. The following procedure will be used to make it unitary. Assume that $\tilde{U}^0(n,m)$ is the original result calculated from Eq. ~22!. Define

$$M(n,m)=$$

Because $M(n,m)$ is positive definite, we can compute the quantity $M^{2\,1/2}(n,m)$. Then, the unitary matrix U

Because the width of the interfacial potential is controlled by $w(r)$ through Eq. ~C1!, to get a sharp interface, it is also necessary to change $w(r)$. Note that $w(r)$ need not be a spherical function. Thus we can expressed $W(k)$ as a general function

$$W\sim k!5 e$$

[33] S. Froyen ~unpublished!.
[34] To save memory, in the evaluation of Eq. ~41!, $H_A^{\mathrm{tot}}(p\delta k\delta,pk)$ was not stored for all $(p\delta k\delta,pk)$. Rather, $H_A^{\mathrm{tot}}(p\delta k\delta,pk)$ can be calculated for each $k\delta$ at a time; thus it does not need a large memory to store it.
[35] K.A. Mader and A. Zunger, Phys. Rev. B **51**, 10 462 ~1995!.
[36] K.A. Mader, L.W. Wang, and A. Zunger, J. Appl. Phys. **78**, 6639 ~1995!.